A MORPHOMETRIC INVESTIGATION OF CRUSTAL SHORTENING STRUCTURES ON MARS. Rachel M. Atkins[1], Paul K. Byrne[1], DelWayne Bohnenstiehl[1], Christian Klimczak[2], [1]Department of Marine, Earth, and Atmospheric Sciences, North Carolina State University, Raleigh, NC 27695, USA, [2]Department of Geology, University of Georgia, Athens, GA 30602, USA (ratkins@ncsu.edu).

Introduction: Throughout its history, Mars has experienced substantial tectonic deformation, as evidenced by its surficial features [1,2]. Crustal shortening has a surface signature of large, asymmetric, positive-relief landforms that exhibit one steep scarp and a gently-sloping backscarp [3]. These surface features are often referred to as "lobate scarps" and are interpreted to be underlain by thrust faults.

Uplift caused by slip along these faults, which are observed to range in length from tens to hundreds of kilometers, produces surface topography on the order of hundreds to thousands of meters. The global distribution of these landforms indicates that they may reflect a planet-scale process such as global contraction resulting from secular interior cooling [e.g., 4].

On the basis of observations from thrust faults on Earth [5,6], these scarps are likely fault-propagation folds that form in proportion to the accumulation of slip along the underlying fault [7]; maximum displacement for an isolated thrust fault is at the center of the fold, decreasing to zero at the tips [3]. An investigation of how the surface displacement changes as a function of distance along the fault can therefore provide a detailed history of fault growth [8]. We investigate these surface changes, along with spatial patterns in fault characteristics, to obtain a more complete understanding about the contractional history and crustal characteristics of Mars.

Methods: We conducted a global survey of crustal shortening structures on Mars, and selected 50 candidate faults with the HRSC–MOLA blended digital elevation model (DEM) (spatial resolution ~200 m/px) and the THEMIS thermal image data set (100 m/px) in ESRI ArcGIS®. Scarps were selected on the basis that their surface rupture was continuously visible and relatively undissected by large impact craters, so as to capture for analysis as complete of a picture of fault morphology and growth as possible. Where possible, we chose relatively spatially isolated structures that displayed little evidence for mechanical interaction with neighboring structures (**Figure 1**).

Scarps were digitized along the surface break of each structure in ArcGIS® and exported for data collection and analysis in MATLAB®. Topographic profiles were extracted perpendicular to each fault trace at 1 km spacing along its length, and used to extract the maximum structural relief along the scarp at each of those points. This spacing reflects an increase in fault relief measurement by an order of magnitude over recent previous studies [e.g., 3], allowing for a more detailed reconstruction of fault growth history. Under the assumption that structural relief corresponds to a minimum estimate for the vertical component of displacement along the underlying fault, surface relief values along the fault were used as minimum throw values along the structure.

These throw values were plotted against fault length to produce fault displacement profiles, which were investigated for evidence of fault segmentation and linkage. The maximum measured throw value for each landform was converted to a maximum fault displacement value (D_{max}) assuming a dip angle of 30° (with $\sin(30°) = \text{throw}/D_{max}$). These values were plotted against fault length to determine a maximum displacement-to-length (D_{max}/L) scaling ratio for each structure, and for the overall data set. Multiple morphometric and spatial characteristics were determined for each fault, including total length, D_{max}, D_{max}/L, strike, latitude and longitude, and geological unit in which the structure occurs based on the global geological map [9]. These properties for each fault were used to look for significant relationships between variables using comprehensive spatial descriptive statistics (e.g., spatial autocorrelation, hotspot, and cluster/outlier analyses in ArcGIS® Pro).

Several of the scarps we investigate are incised by valley networks that are oriented down-dip [3]. On the basis of superposition relations, this orientation supports the interpretation that the valleys post-date the uplift. Therefore, impact craters on and surrounding these faults were classified as either pre- or post-dating the deformation by their timing relationships with valley networks, and by the degradation state of craters emplaced on the scarp but not in direct contact with a valley. Absolute model surface ages were calculated with Craterstats 2.0 [10], using the production function from ref. [11] and the chronology function from Hartmann and Neukum (2001) [12].

Findings: The scarps investigated for this project range in length from 35–715 km, with maximum surface displacements of 85 m to as much as 2.6 km. D_{max}/L ratios for our fault population (assuming a planar fault geometry with a dip angle of 30°) vary from 5.0×10^{-4} to 2.0×10^{-2}, with a mean ratio of 6.2×10^{-3}. This mean falls within the published range of calculated D_{max}/L ratios for other Martian thrust faults of 2×10^{-3} to 7.5×10^{-3} [13,14]. In contrast to earlier studies, we include far more structures and assess them in greater detail.

Our findings also show a statistically significant difference between D_{max}/L ratios of faults situated in the northern lowlands and southern uplands, with higher ratios for the latter population (mean $D_{max}/L = 9.2\times10^{-3}$) compared with those in the north (mean $D_{max}/L = 3.1\times10^{-3}$); 99% confidence ranges are (2.4×10^{-3}, 2.0×10^{-2}) and (5.0×10^{-4}, 8.1×10^{-3}), respectively. This finding indicates that faults in the southern hemisphere are accommodating more surface displacement for a given length than their counterparts in the northern lowlands. (**Figure 2**).

For one such structure, located at 55.4° S, 150.1° W, we find a model age of 3.8 Ga for the pre-uplift crater population and 3.7 Ga for that crater population formed post-uplift. (We do not quote formal errors for these age values.) These ages are not statistically different from each other, which leads us to conclude that this channel network formed very soon after the scarp had developed, with both being in place by the late Noachian/early Hesperian.

Outlook: Results from our study show that our globally distributed population of large-scale thrust faults have D_{max}/L ratios consistent with previous studies, but, importantly, that there are statistically significant differences in D_{max}/L ratios for scarps in the northern lowlands and southern uplands. This finding may indicate differences in crustal structure between the northern and southern hemispheres that have influenced the nature and style of faulting, and the amount of surface displacement that can be accommodated for a given fault length.

Our derived Martian D_{max}/L ratios are also comparable to the range of reported values for Mercury (9.6×10^{-3} to 7.1×10^{-3}) [15], a world with the same surface gravitational acceleration as Mars. Of note, our Martian D_{max}/L values for the southern hemisphere most closely match those for Mercury, suggesting that crustal deformation processes in the older, southern uplands resemble those in Mercury's ancient "intercrater plains" [7,15]; both terrain types likely comprise volcanic and magmatic rocks mixed with impact-generated deposits. The detailed analysis of crustal shortening on Mars therefore offers not only new insight into the geological and tectonic evolution of that planet, but of how tectonic deformation operates on rocky, one-plate worlds in general. Moreover, continued assessment of timing relations of scarp formation will lead to firmer constraints on the timing of major crustal shortening, and in turn the thermal evolution, of Mars.

References: [1] Solomon S. C. (1978) *Geophysical Research Letters, 5*, 461–464. [2] Hauck S. A. II and Phillips, R. J. (2002) *JGR, 107*, 1–19. [3] Klimczak C. et al. (2018) *JGR Planets, 123*, 1973–1995. [4] Nahm A. L. and Schultz R. A. (2011) *Icarus, 211*, 389–400. [5] Suppe, J. and Medwedeff D. A. (1990) *Eclogae Geologicae Helvetiae*, 454, 409–454. [6] Wickham J. (1995) *Journal of Structural Geology, 17*, 1293–1302. [7] Byrne et al. (2018) *Cambridge Univ. Press*, 249–286. [8] Cowie P. and Scholz C. (1992) *Journal of Structural Geology, 14*, 1149–1156. [9] Tanaka et al. (2014) *Geologic Map of Mars: U.S. Geological Survey Scientific Investigations Map 3291*. [10] Michael G. and Neukum G. (2010) *Earth and Planetary Science Letters, 3*, 223–229. [11] Ivanov B. (2001) *Space Science Reviews, 96*, 87–104. [12] Hartmann W. and Neukum G. (2001) *Space Science Reviews, 96*, 165-194. [13] Watters et al. (2000) *Geophysical Research Letters, 27*, 3659–3662. [14] Schultz, R. et al. (2006) *Journal of Structural Geology, 28*, 2182–2193. [15] Byrne et al. (2014) *Nature Geoscience, 7*, 301–307.

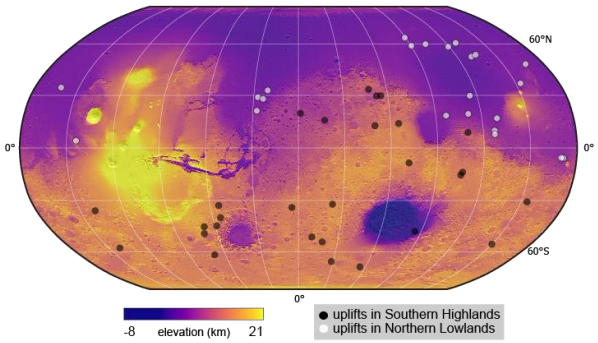

Figure 1. A global map of Mars with the locations of the 50 faults we consider here.

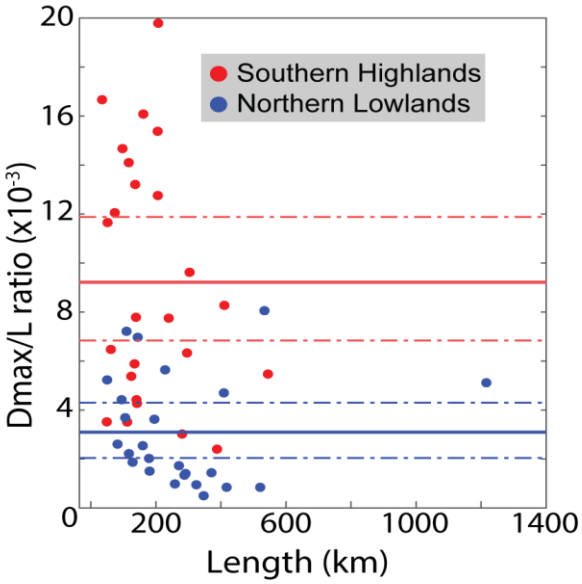

Figure 2. D_{max}/L ratios for the investigated 50 faults showing that faults in the northern lowlands (n = 32) have statistically significantly lower ratios (3.1×10^{-3}) than faults in the southern highlands (n = 28, 9.2×10^{-3}). The dashed lines show 99% confidence intervals, computed by bootstrapping 10,000 means for each population, and show no overlap.